IEEE Access
Multidisciplinary | Rapid Review | Open Access Journal

Received July 8, 2020, accepted July 18, 2020, date of publication July 27, 2020, date of current version September 30, 2020.

Digital Object Identifier 10.1109/ACCESS.2020.3012091

Design, Mathematical Modeling and Force Control for Electro-Hydraulic Servo System With Pump-Valve Compound Drive

BIN YU[1,2], (Member, IEEE), QIXIN ZHU[1], JING YAO[1,2], JUNXIAO ZHANG[1], ZHIPENG HUANG[1], ZHENGGUO JIN[1], AND XIANGJI WANG[1]

[1]School of Mechanical Engineering, Yanshan University, Qinhuangdao 066004, China
[2]School of Mechanical Engineering, Nanjing Institute of Technology, Nanjing 211167, China

Corresponding author: Jing Yao (jyao@ysu.edu.cn)

This work was supported in part by the National Natural Science Foundation of China under Grant 51975506, in part by the National Key Research and Development Project of China under Grant 2018YFB2000701, in part by the Science and Technology Research Project of Colleges and Universities in Hebei Province under Grant BJ2020016, and in part by the Hebei Province Introduced Foreign Intelligence Project under Grant 2020-19.

ABSTRACT Each joint of hydraulic drive legged robot adopts highly integrated electro-hydraulic servo system, and the system has two common forms, namely, valve-controlled cylinder system and pump-controlled cylinder system. The former has a large energy loss, which restricts the endurance of the legged robot in the field. Although the latter has the advantages of energy saving and high efficiency, the overall response ability of control system is unsatisfied. In this paper, a novel pump-valve compound drive system (PCDS) is designed. It combines the advantages of pump-controlled cylinder system and valve-controlled cylinder system, which can not only effectively reduce the energy loss of the system, but also ensure the electro-hydraulic servo system of the robot joint has the ideal response ability. This paper consists of three parts. In the first part, the mathematical model of nonlinear force control of PCDS is established, which takes into account the pressure-flow nonlinearity of servo valve, the asymmetry of servo cylinder and the complexity and variability of load. So this model has a high accuracy. In the second part, On the basis of the above model, a force control method combining tracking error compensation and load compensation control is designed. And this control method can improve the control precision of the robot. In the third part, the performance of the designed control method is verified by experiments. The experiments show that the designed force control method can effectively reduce the influence of external position disturbance on the tracking accuracy of the force control system and improve the control accuracy of the robot joint movement.

INDEX TERMS Legged robot, electro-hydraulic, pump-valve compound drive system (PCDS), mathematical modeling, force control.

I. INTRODUCTION

In recent years, researchers in various countries have made in-depth studies on the field of mobile robots. Mobile robots can be divided into wheeled robot [1], tracked robot [2], legged robot [3], snake-like robot [4], spherical robot [5], etc. The legged robot is designed with a structure similar to the creature with feet in natural, and this kind of robot has the characteristics of discontinuous support, which has good adaptability to unknown and unstructured environment. Especially in recent years the legged robot has been combined with hydraulic system, which makes the legged robot drive by hydraulic system more suitable for the missions such as detection, transportation, rescue and military assistance in complex environments or the wild. Most of the drive units of hydraulic drive legged robot use valve-controlled throttling system, but its energy utilization rate is still very low. The pump-control system with volumetric control can effectively improve the endurance of the robot, but its response speed is low and the control accuracy is unsatisfied [6], [7]. Therefore, it is urgent to study a pump-valve compound control system and its control methods.

In recent years, scholars from many countries have carried out a lot of research on the force control system of hydraulic

The associate editor coordinating the review of this manuscript and approving it for publication was Yingxiang Liu.

and motor and they have developed a variety of control methods, such as fuzzy logic control [8], intelligent control [9], quantitative feedback control [10], [11] and robust control [12], [13]. Endo *et al.* [14] studied a simple boundary feedback controller composed of the bending moment at the root of the flexible arm and its time derivative, which solved the force control problem of the constrained single-bar flexible arm. Jiao and Yao [15] studied a nonlinear adaptive robust inverse step force controller based on discontinuous projection to improve the robustness of force control of hydraulic load simulator. Wang *et al.* [16] studied the flow compensator, speed compensator and internal model controller to improve the dynamic performance of the force control system. Aimed at the problems of environmental constraints and incorrect modeling, Cao *et al.* [17] adopted a fast terminal sliding mode control method and proposed an adaptive finite time motion/force control method, Yao *et al.* [18] proposed a nonlinear adaptive robust force control, which achieves a guaranteed transient performance and final tracking accuracy in the presence of both parametric uncertainties and uncertain nonlinearities; in the absence of uncertain nonlinearities, the scheme also achieves asymptotic tracking performance. In addition, many researchers such as Truong and Ahn [19] and Nakkarat and Kuntanapreeda [20] have conducted a lot of research on electro-hydraulic servo force control system and obtained relevant research results. A variety of control methods are used in the optimization of the control performance of the force control system in the above-mentioned references, and the control effect is very good. However, due to the complexity of the control models, most of their research work are simulation analysis or are only completed in the laboratory, and the diversity of the given signals and the complexity of the environment load are not taken into consideration. Therefore, the effectiveness of the force control method is still to be further verified in engineering practice.

The main contribution of this paper is as follows:

- A novel pump-valve compound drive system (PCDS) is designed, which combines the advantages of pump-controlled cylinder system and valve-controlled cylinder system.
- The mathematical model of nonlinear force control of PCDS is established, which takes into account the pressure-flow nonlinearity of servo valve, the asymmetry of servo cylinder and the complexity and variability of load.
- A force control method combining tracking error compensation and load compensation control is designed. It has been proved by experiment that the control method can effectively reduce the influence of external position disturbance on the tracking accuracy.

To sum up, the organization of this paper is as follows: in the first section, an electro-hydraulic servo system with pump-valve compound drive is designed. In this system, through the servo valve installed at both ends of the pump port to supply or drain the two cavities of the asymmetrical cylinder, the pressure closed-loop control is realized and combined with the force closed-loop control of the pump control loop. It not only reduces the problem of high energy loss of single valve-controlled cylinder system, but also makes up for the problem of low response and low precision of single pump-controlled cylinder system to a certain extent. When it is applied to the legged robot, it will improve the response speed, control accuracy and endurance of the robot in the field. In the second section, in order to facilitate the design of PCDS controller, the mathematical model of the key components of the system is established, and the whole mathematical model of the system is formed. In the third section, aiming at the problem of poor tracking performance caused by the inherent characteristics of force control of PCDS, a compound control method including tracking error compensation control method and load compensation control method is proposed. Finally, the performance of the proposed compound control method is verified on the PCDS test platform.

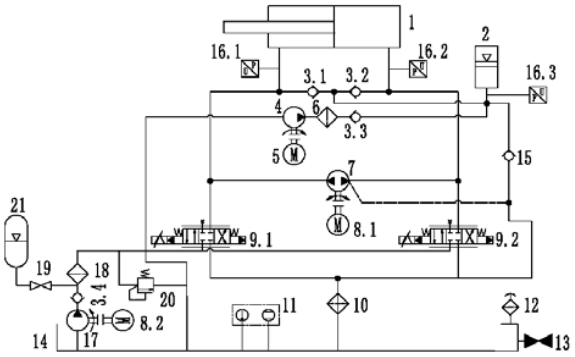

1-Servo hydraulic cylinder 2Oil tank 3-Check valve 4-Filling pump 5-Oil filling motor 6-Filter 7-Two-way quantitative gear pump 8-Servo motor 9-Bypass servo valve 10-Cooler 11-Liquid level thermometer 12-Air filter 13-Low pressure ball valve 14-Oil tank 15-High pressure check valve 16-Pressure sensor 17-One-way quantification Gear pump 18-High pressure gear pump 19-Stop valve 20-Relief valve 21-Energy accumulator

FIGURE 1. Hydraulic schem atic diagram of PCDS.

II. DESIGN AND WORKING PRINCIPLE OF PCDS

PCDS is mainly composed of pump control loop, valve control loop and oil-addition loop, as shown in Figure 1. In the pump control loop, two-way quantitative gear pump 7 is drive by servo motor 8.1 to realize bi-directional rotation and then control the action of asymmetrical cylinder 1. The actual force signal is calculated by the pressure sensor 16.1 and 16.2, and the force closed-loop control system is realized. In the valve control loop, the asymmetrical cylinder pressure closed-loop control system is composed of bypass servo valve 9.1 and pressure sensor 16.1. A rodless cavity pressure closed-loop control system of the asymmetrical cylinder is composed of bypass servo valve 9.2 and the pressure

sensor 16.2. According to the pressure, the bypass servo valve 9.1 and 9.2 are controlled to supply or drain oil to the two-cavity volume of the asymmetrical cylinder, so as to realize the pressure closed-loop control with high precision and high response to the two-cavity volume of the asymmetrical cylinder. The oil supplyment process is divided into the main supplyment process and the auxiliary supplyment process. The main filling process is supplemented by the pressure-controlled bypass servo valve, and it needs the one-way quantitative gear pump 17 drive by the servo motor 8.2 to provide the oil source for the system. The auxiliary filling process is conducted through the pressurized tank 2 and three one-way valves 3.1, 3.2 and 3.3. Screw pump 4 is drive by oil filling motor to supply oil source of pressurized oil tank 2, and the pressure of pressurized oil tank is measured by pressure sensor 16.3 to maintain the pressure of pressurized oil tank at 5bar, and filter 6 is added to ensure oil cleaning.

In order to suffice the force control performance with high response, high precision and energy saving of PCDS, three closed-loop controls should be realized in the system, namely, force control closed loop for the pump-control loop, pressure-controlled closed loop for the rodless cavity of asymmetrical cylinder, pressure controlled-closed loop for the rod cavity of asymmetrical cylinder. The control principle block diagram of the system is shown in Figure 2.

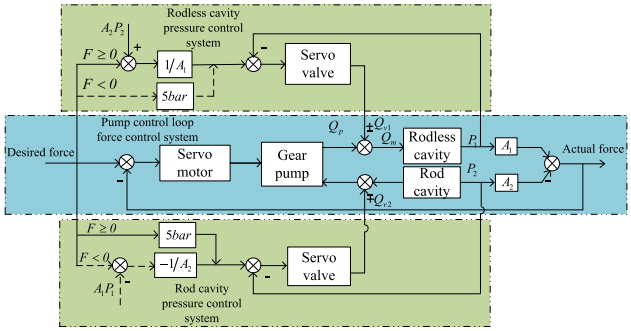

FIGURE 2. Force control principle block diagram of PCDS.

In Figure 2, P_1 is the pressure of the rodless cavity of asymmetrical cylinder, P_2 is the pressure of the rod cavity of asymmetrical cylinder. Q_{v1} is the flow rate of the rodless cavity of servo valve, Q_{v2} is the flow rate of the rod cavity of servo valve, Q_p is the flow rate of the gear pump, and Q_m represents the sum of the flow rate of the pump control loop and the valve control loop. Combined with Figure 2, the principle of PCDS is described in detail as follows:

When the load force on the system is $F > 0$, the rodless cavity of the asymmetrical cylinder is a high-pressure cavity, and the pressure sensor measures the pressure signal of the rodless cavity of the asymmetrical cylinder. Compared the desired input pressure signal, the error signal is obtained, which is output to the servo valve through the relevant controller. Furthermore, the opening of the valve is adjusted to supply or drain oil for the rodless cavity of the asymmetrical cylinder, so as to realize the pressure closed-loop control of the rodless cavity of the asymmetrical cylinder. At this time, the rod cavity of the asymmetrical cylinder is low-pressure cavity, and because of the automatic oil supplyment in the oil supply loop, the pressure sensor measures the pressure signal of the rodless cavity to obtain the error signal by comparing with the desired input pressure. Furthermore, the opening of the valve is adjusted to supply or drain oil for the rod cavity of the asymmetrical cylinder, and the pressure of the cavity is maintained in the pressure closed-loop control of 5 bar. When the load force $F < 0$, the rod cavity of the asymmetrical cylinder is high-pressure cavity, and the rod cavity is low-pressure cavity. The working principle of each servo valve is contrary to that of the system with load force $F > 0$, so it is necessary to describe in detail.

On the basis of the asymmetrical cylinder two-cavity pressure control system, the actual output force of the force control system is obtained by calculating the two-cavity pressure of the asymmetrical cylinder, and the force error signal is obtained by comparing with the desired force. Through the relevant controller, the output force error signal is delivered to the servo motor, which controls the rotation of the gear pump, and finally the PCDS force control is realized.

As can be seen from Figure 2, PCDS force control can be realized through the joint action of pump control loop and valve control loop. Therefore, the PCDS force servo control system is a multi-input control system essentially.

As a multi-input control system, it is necessary to discuss the contribution of pump control loop and valve control loop to the output force of the system. In order to facilitate a clear discussion of the contribution of each loop, this paper only discusses the situation that the rodless cavity of asymmetrical cylinder is at high pressure state, and ignores the flow rate variation of the low-pressure cavity. Q_v is the flow of the high-pressure cavity through the servo valve. The larger value of Q_p or Q_v in Q_m , the greater its effect is. According to the different output flow conditions of the pump control loop and the valve control loop, the system can be divided into the several situations as follows:

Firstly, when $Q_p \neq 0$ and $Q_v \neq 0$, the valve control loop and the pump control loop adjust the force control system together, then the system is in the pump-valve compound drive mode.

If the servo valve is in the oil drain state, the flow rate of the asymmetrical cylinder is equal to the difference between the flow rate of the pump control loop and the flow rate of the valve control loop, namely, $Q_m = Q_p - Q_v$. The system is in drain drive mode.

If the servo valve is in the oil supplyment state, the flow rate of the asymmetrical cylinder is equal to the sum of the flow rate of the pump control loop and the flow rate of the valve

control loop, namely, $Q_m = Q_p + Q_v$.At this time, the system is in the drive mode of supplying oil with valve.

Secondly, when $Q_p \neq 0$ and $Q_v \neq 0$, the gear pump adjusts the force control system separately, and the system is in the traditional pump control mode. Because of the asymmetrical flow rate problem caused by the asymmetrical cylinder, there is no servo valve for draining oil, so it doesn't conform to reality.

Thirdly, when $Q_p = 0$ and $Q_v \neq 0$, the servo valve adjusts the force control system separately, and the system is in the traditional valve-controlled mode.

As the joint actuator of legged robot, the force control system should adopt the pump-valve compound drive mode, in which the servo valve can not only supply oil but also drain oil to suffice the response requirements of the robot in high-speed motion. The force servo control with high precision, high response and energy saving is realized. Therefore, this paper aims at the pump-valve compound drive mode to carry out a serial of research.

III. NONLINEAR MATHEMATICAL MODELING OF PCDS

This section establishes the mathematical model of the key components of PCDS, including servo motor, gear pump, oil supply loop and asymmetrical cylinder. The mathematical model of experimental platform of PCDS loading system and related high-precision position control have been carried out in the author's previous research [21]–[23]. Due to space limitation, it doesn't be introduced repeatedly.

A. MATHEMATICAL MODEL OF SERVO MOTOR

The voltage balance equation of servo motor is shown as follow:

$$U_c = E + L\frac{\mathrm{d}i}{\mathrm{d}t} + Ri \tag{1}$$

where, E is back electromotive force, i is armature current, L is armature inductance, R is armature winding resistance.

The reverse electromotive force of the servo motor is shown as follows:

$$E = K_c w \tag{2}$$

where, K_c is electromagnetic torque system, w is servo motor speed.

$$T_e = K_t i \tag{3}$$

where, K_t is torque coefficient of servo motor, T_e is electromagnetic torque of servo motor.

The servo motor and the gear pump are directly connected, and the torque balance equation is shown as follows:

$$T_e = J\dot{w} + B_p w + T_L \tag{4}$$

where, J is conversion to moment of inertia of servo motor shaft, B_p is viscous friction coefficient of servo motor, T_L is external load torque of servo motor.

To realize the accurate control of servo motor, three closed loops control is usually used, which are current closed loop, speed closed loop and position closed loop from inside to outside respectively. The torque control of servo motor adopts current closed loop, and the its dynamic response is the fastest [24]. This paper mainly focuses on the force control of PCDS, and takes into account the response of the system, so the servo motor in the system adopts torque control mode. The current loop controller K_{PI} can set the control parameters of the current loop to realize the accurate control of the servo motor torque. The transfer block diagram of the servo motor torque control system is shown in Figure 3.

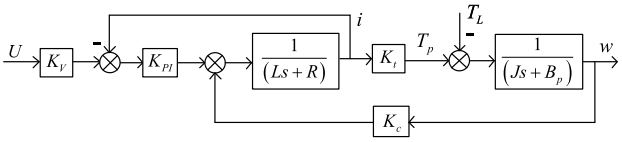

FIGURE 3. The transfer block diagram of the servo motor torque control system.

In Figure 3, K_V is a voltage and current conversion coefficient, the influence of the external disturbance torque of the servo motor is ignored, and the open-loop transfer function between the input voltage and the output speed of the servo motor is obtained as follows:

$$\frac{w}{U} = \frac{K_V K_{PI} K_t}{LJ^2 s^3 + RJ^2 s^2 + J\left(K_c K_t + K_{PI} K_f\right) s} \tag{5}$$

B. MATHEMATICAL MODEL OF GEAR PUMP

When the gear pump is positive rotation, the internal and external leakage of the gear pump are considered, the flow-pressure relationship is shown in Figure 4.

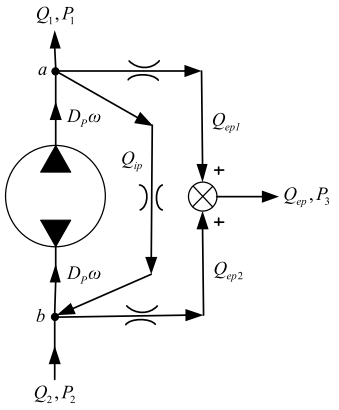

FIGURE 4. Diagram of flow- pressure relationship of gear pump.

The flow equations of gear pumps are shown as follows:

$$Q_1 = D_p w - Q_{ip} - Q_{ep1} \tag{6}$$

$$Q_2 = D_p w - Q_{ip} - Q_{ep2} \tag{7}$$

where, D_p is the displacement of gear pump, W is the speed of gear pump, Q_{ip} is the internal leakage flow of gear pump, Q_{ep1} is the external leakage flow of gear pump at point a, Q_{ep1} is the external leakage flow of gear pump at point b.

The nonlinear problems of leakage flow and pressure are considered, the expression can be obtained as follows:

$$Q_{ip} = K_{ip}(P_1 - P_2) \tag{8}$$
$$Q_{ep1} = K_{im}(P_1 - P_3) \tag{9}$$
$$Q_{ep2} = K_{im}(P_2 - P_3) \tag{10}$$

where, K_{ip} is the internal leakage coefficient of gear pump, K_{im} is the external leakage coefficient of gear pump, P_1 is the pressure of gear pump at point a, P_2 is the pressure of gear pump at point b, P_3 is the pressure of gear pump at point c. Pressure connecting to the external tank directly is 0 bar.

C. MATHEMATICAL MODEL OF FILLING LOOP

1) MATHEMATICAL MODEL OF PRESSURIZED FUEL TANK AND ONE-WAY VALVES

The PCDS is a closed system, which needs to supply oil to the system through the oil supply loop composed of oil tank, check valve and servo valve. Its main functions are shown as follows:

1) Maintaining a constant pressure in the low-pressure cavity of asymmetric cylinder. 2) Supplying the hydraulic oil's leakage of the force control system. 3) Preventing cavitation problems caused by high-frequency vibration of the system.

In the modeling of the traditional pump-control system, the oil supplyment link is often ignored, resulting in a certain error in the analysis results. Therefore, the relationship between flow rate and pressure is analyzed as shown in Figure 5.

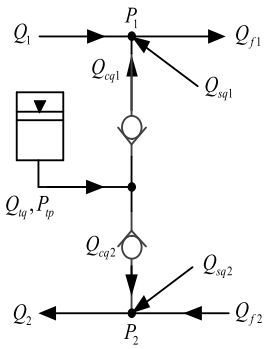

FIGURE 5. Diagram of flow-pressure relationship between low pressure fuel tank and check valve oil supplyment.

The flow equations of each link are as follows:

$$Q_{f1} = Q_1 + Q_{cq1} - Q_{sq1} \tag{11}$$
$$Q_{f2} = Q_2 - Q_{cq2} + Q_{sq2} \tag{12}$$
$$Q_{tq} = Q_{cq1} + Q_{cq2} \tag{13}$$

where, Q_{cq1} is check valve flow connected with asymmetrical cylinder rodless cavity, Q_{cq2} is check valve flow connected with asymmetrical cylinder rod cavity, Q_{sq1} is servo valve flow connected with asymmetrical cylinder rodless cavity, Q_{sq2} is servo valve flow connected with asymmetrical cylinder rod cavity, Q_{tq} is the flow out of the pressurized fuel tank.

Taking the check valve as the throttle port model, the expression can be obtained as follows:

$$Q_{cq1} = \begin{cases} K_{cp}\sqrt{P_{tp} - P_1} & w \geq 0 \\ K_{cp}\sqrt{P_1 - P_{tp}} & w < 0 \end{cases} \tag{14}$$

$$Q_{cq2} = \begin{cases} K_{cp}\sqrt{P_{tp} - P_2} & P_{tp} \geq P \\ 0 & P_{tp} < P \end{cases} \tag{15}$$

where, P_{tp} is the output pressure of the pressurized fuel tank, K_{cp} is the flow pressure coefficient of check valve.

Due to the complexity of modeling for pressurized fuel tank and the fact that pressurized fuel tank and energy accumulator have similar functions, this paper uses the mathematical model of energy accumulator instead of the mathematical model of pressurized fuel tank. The equation of input flow and output pressure of pressurized fuel tank are shown as follows:

$$P_{tp} = P_{gp} V_{gv}^k \Big/ \left[V_{gv} - \int q_{tp} \mathrm{d}t \right]^k \tag{16}$$

where, P_{gp} is the initial pressure of pressurized fuel tank, V_{gv} is the initial volume of gas in the pressurized fuel tank, k is the polytropic index of nitrogen, generally 1.0∼1.4.

2) FLOW EQUATIONS OF SERVO VALVE

Servo valves installed on the two sides of the asymmetric cylinder will supply or drain oil from the two cavities of the asymmetric cylinder. The transfer function of servo valve can be simplified to second order oscillation systems. The transfer function of servo valve input voltage and displacement of the valve core is shown as follows:

$$\frac{X_v}{U_g} = \frac{K_a K_{xv}}{\frac{s^2}{\omega^2} + \frac{2\zeta}{\omega} s + 1} \tag{17}$$

where, K_a is the gain of servo valve power amplifier, K_{xv} is the gain of servo valve, ζ is the damping ratio of servo valve, ω is the natural frequency of servo valve.

For the convenience of calculation, the slide valve level of servo valve is equivalent to an ideal zero-opening four-way slide valve, and the flow equation of four-way slide valve is established. The flow of asymmetrical cylinder rodless cavity is shown as follows:

$$Q_{sq1} = \begin{cases} K_d x_{v1}\sqrt{p_s - p_1} & x_{v1} > 0 \\ K_d x_{v1}\sqrt{p_1 - p_0} & x_{v1} < 0 \end{cases} \tag{18}$$

The inlet flow rate of servo valve connected with rod cavity is shown as follows:

$$Q_{sq1} = \begin{cases} K_d x_{v2}\sqrt{p_s - p_2} & x_{v2} > 0 \\ K_d x_{v2}\sqrt{p_2 - p_0} & x_{v2} < 0 \end{cases} \tag{19}$$

where, K_d is equivalent flow coefficient, x_{v1} is the displacement of the servo valve connected with the rodless cavity of the asymmetric cylinder, x_{v2} is the displacement of the servo valve connected with the rod cavity of the asymmetric cylinder, p_s is the supply oil pressure of servo valve, p_1 is

the pressure of asymmetrical cylinder rodless cavity, p_2 is the pressure of asymmetrical cylinder rod cavity, p_0 is the return oil pressure of system, which takes 0 bar.

The expression of the equivalent flow coefficient is shown as follows:

$$K_d = C_d W \sqrt{\frac{2}{\rho}} \tag{20}$$

where, C_d is the flow coefficient of servo valve throttle orifice, W is area gradient, ρ is hydraulic oil density.

D. MATHEMATICAL MODEL OF ASYMMETRICAL CYLINDER

1) FLOW CONTINUITY EQUATION

The inlet flow of asymmetrical cylinder rodless cavity and the volume of oil-in cavity are shown as follows:

$$\begin{cases} Q_{f1} = A_1 \dfrac{\mathrm{d}x_p}{\mathrm{d}t} + C_{im}(p_1 - p_2) + \dfrac{V_1}{\beta_e}\dfrac{\mathrm{d}p_1}{\mathrm{d}t} \\ V_1 = V_{01} + A_1 x_p \end{cases} \tag{21}$$

The oil return flow of asymmetrical cylinder rod cavity and the volume of oil-out cavity are shown as follows:

$$\begin{cases} Q_{f2} = A_2 \dfrac{\mathrm{d}x_p}{\mathrm{d}t} + C_{im}(p_1 - p_2) - \dfrac{V_2}{\beta_e}\dfrac{\mathrm{d}p_2}{\mathrm{d}t} \\ V_2 = V_{02} - A_2 x_p \end{cases} \tag{22}$$

where, A_1 is the effective area of asymmetrical cylinder rodless cavity, A_2 is the effective area of asymmetrical cylinder rod cavity, x_p is the piston displacement of asymmetrical cylinder, C_{im} is the internal leakage coefficient of asymmetrical cylinder, β_e is the elastic modulus of effective volume, V_{01} is the initial volume of asymmetrical cylinder rodless cavity, V_{02} is the initial volume of asymmetrical cylinder rod cavity.

In the initial volume of rodless cavity and rod cavity of asymmetric cylinder, the volume variation of working cavity, connecting pipe and asymmetric cylinder of gear pump need to be considered, and the expressions can be obtained as follows:

$$\begin{cases} V_{01} = V_{P1} + V_{g1} + A_p L_0 \\ V_{02} = V_{P2} + V_{g2} + A_p (L - L_0) \end{cases} \tag{23}$$

where, V_{P1} is the volume of working cavity of gear pump connected with asymmetrical cylinder rodless cavity, V_{P2} is the volume of working cavity of gear pump connected with asymmetrical cylinder rod cavity, V_{g1} is the pipe volume connected the gear pump and the asymmetric cylinder rodless cavity, V_{g2} is the pipe volume connected the gear pump and the asymmetric cylinder rod cavity, L is the total piston displacement of asymmetrical cylinder, L_0 is the initial position of asymmetrical cylinder.

2) FORCE BALANCE EQUATION

Since the asymmetric cylinder is affected by inertia force, viscous damping force, elastic force and any external load force, the balance equation of the output force and load force of the asymmetric cylinder are shown as follows:

$$\begin{aligned} F_g &= A_1 p_1 - A_2 p_2 \\ &= m_t \frac{\mathrm{d}(x_p - x_L)^2}{\mathrm{d}t} + B_p \frac{\mathrm{d}(x_p - x_L)}{\mathrm{d}t} + K(x_p - x_L) + F_f \end{aligned} \tag{24}$$

where, m_t is the total mass converted to the asymmetric cylinder piston, including the load mass block, piston, connection pipe and the oil in asymmetric cylinder, K is the load stiffness of asymmetric cylinder, B_p is the damping coefficient of load and asymmetric cylinder, F_f is the coulomb friction of load and asymmetric cylinder, x_L is position disturbance acting on the asymmetric cylinder piston.

E. MATHEMATICAL MODEL OF PRESSURE SENSOR

The sampling frequency of the selected pressure sensor is more than 5 times that of the control system. The transfer function of sensor is equivalent to a proportional link, and the transfer function between the feedback voltage and the oil pressure is shown as follows:

$$\frac{U_p}{P} = K_{ps} \tag{25}$$

where, K_{ps} is the gain of pressure sensor, P is the pressure signal measured by the pressure sensor.

Combined with Eqs. (1) to (25), the whole mathematical model of PCDS force control can be established, in which the pump control loop and the valve control loop adopt PID controller, as shown in Figure 6.

IV. THE DESIGN OF PCDS FORCE CONTROLLER

The second section gives the overall mathematical model of PCDS force control. This mathematical model is based on the traditional PID controller, but the traditional PID controller can't meet the requirements of high-performance force control for robot systems in practical engineering applications. Moreover, due to the inherent characteristics of PCBS force control, the tracking performance of the system is poor, so the control precision and robustness need to be improved urgently. In this section, the pump control loop and valve control loop are considered separately to study the integrated control method of each loop. This control method includes tracking error compensation control method and load compensation control method. Combining pump control loop and valve control loop control method, it constitutes the compound control method of PCDS, so as to improve system force control performance and improve system engineering application value.

A. LOAD COMPENSATION CONTROL METHOD FOR FORCE CONTROL SYSTEM

This section will design the load compensation control method of each loop from the principle of pump control loop and valve control loop to eliminate the influence of external position disturbance on the force control system.

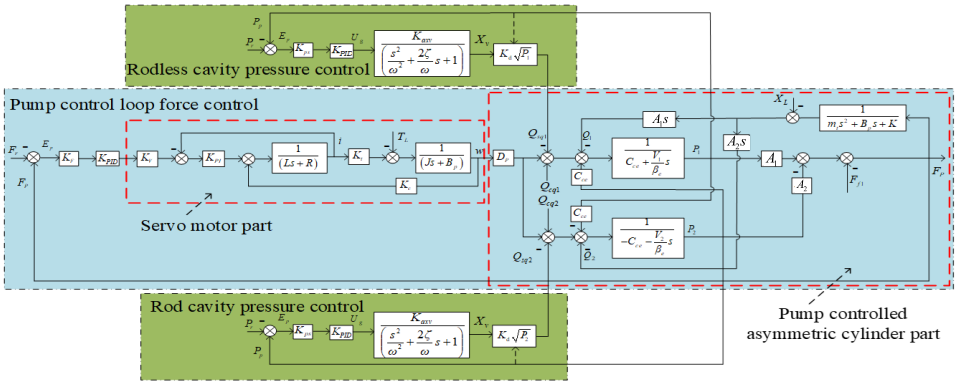

FIGURE 6. The overall mathematical model of the PCDS force control.

1) VALVE CONTROL LOOP LOAD COMPENSATION CONTROL METHOD

When the external position disturbance X_L is applied to PCDS, it will affect the pressure of two asymmetric cavities. If the pressure error of the two cavities is close to zero, the system's force control function is better. In this section, the load compensation controller is designed with the goal of two-cavity pressure error approaching zero.

a: LOAD COMPENSATION CONTROL METHOD FOR THE RODLESS CAVITY PRESSURE CONTROL SYSTEM

Combined with PCDS control schematic in Figure 2 and the transfer block diagram of pump-valve compound drive force control system in Figure 6, the closed-loop control schematic diagram of the rodless cavity pressure can be obtained as shown in Figure 7.

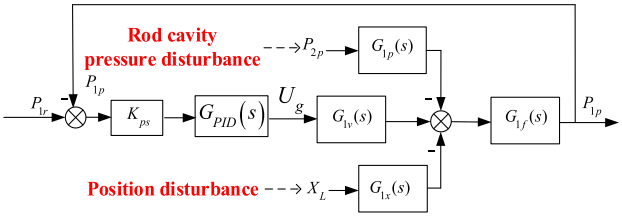

FIGURE 7. The schematic diagram of closed-loop control of rodless cavity pressure.

In Figure 7, P_{1r} is the desired pressure of rodless pressure control system, P_{1p} is the actual pressure of rodless pressure control system, P_{2p} is the actual output pressure of the asymmetrical cylinder rodless cavity, $G_{1v}(s)$ and $G_{1f}(s)$ are the transfer functions of each part of the closed-loop control system of the rodless cavity's pressure, $G_{1x}(s)$ is the transfer function of external disturbance position acting on the pressure control system, $G_{1p}(s)$ is the transfer function of the rod cavity pressure P_{2p} acting on the system.

For the sake of calculation, some equations in Figure 6 are transformed as follows:

$$K_1 = \begin{cases} K_d\sqrt{p_s - p_1} & x_{v1} \geq 0 \\ K_d\sqrt{p_1 - p_0} & x_{v1} < 0 \end{cases} \tag{26}$$

$$K_2 = \begin{cases} K_d\sqrt{p_2 - p_0} & x_{v2} \geq 0 \\ K_d\sqrt{p_s - p_2} & x_{v2} < 0 \end{cases} \tag{27}$$

Combining with Eqs. (26) and (21), the rodless cavity pressure P_{1p} can be obtained as follows:

$$P_1 = \frac{Q_{sq1} + C_{ce}P_2 - A_1X_Ps}{C_{ce} + \frac{V_1 s}{\beta_e}} \tag{28}$$

Denoting $U_g = 0$ and $P_{2p} = 0$, according to Figure 7, $G_{1x}(s)G_{1f}(s)$ can be obtained, the following equation can be obtained by inserting Eq. (28) to Eq. (23), (29), as shown at the bottom of the next page.

Denoting $U_g = 0$ and $X_L = 0$, according to Figure 7, $G_{1p}(s)G_{1f}(s)$ can be obtained as (30), shown at the bottom of the next page.

Donating $P_2 = 0, P_{2p} = 0$ and $X_L = 0$, according to Figure 7, $G_{1v}(s)G_{1f}(s)$ can be obtained as (31), shown at the bottom of the next page.

According to Figure 6, the following equation can be obtained.

$$G_{1x}(s) = A_1\left(m_t s^3 + B_p s^2 + Ks\right) \tag{32}$$

The following equations can be obtained by combining with Eqs. (29) to (32)

$$G_{1v}(s) = \frac{K_{axv}K_1X_v(m_t s^2 + B_p s + K)}{\left(\frac{s^2}{\omega^2} + \frac{2\zeta}{\omega}s + 1\right)} \tag{33}$$

$$G_{1p}(s) = m_t C_{ce}s^2 + \left(B_p C_{ce} + A_1A_2\right)s + KC_{ce} \tag{34}$$

$$G_{1f}(s) = \frac{1}{\frac{V_1 m_t}{\beta_e}s^3 + \left(C_{ce}m_t + \frac{V_1 B_p}{\beta_e}\right)s^2 + \left(A_1^2 + C_{ce}B_p + \frac{V_1 K}{\beta_e}\right)s + KC_{ce}} \tag{35}$$

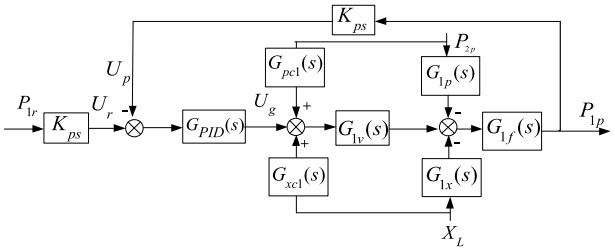

FIGURE 8. The schematic diagram of load compensation control of rod cavity pressure control.

As can be seen from Figure 7, when the external position disturbances X_L and the rod cavity pressure P_{2p} act on the closed-loop control system of rodless cavity, the output pressure of the system will be affected to a certain extent. Since the external position disturbance and the pressure of rod cavity can be measured by the sensor, the designed position load compensation controller $G_{xc1}(s)$ and pressure load compensation controller $G_{pc1}(s)$ can eliminate the influence of the external disturbance signal on the system through the feedforward channel, before it has a negative impact on the system. The schematic diagram of rod cavity's pressure control compensation is obtained, as shown in Figure 8.

The assumptions are made as follows in Figure 8.

$$G_{pc1}(s) = \frac{G_{1p}(s)}{G_{1v}(s)} \tag{36}$$

$$G_{xc1}(s) = \frac{G_{1x}(s)}{G_{1v}(s)} \tag{37}$$

Combining Eqs. (33) and (34), the load compensation controller of system pressure can be expressed as follows:

$$\begin{aligned} G_{pc1}(s) &= \frac{G_{1p}(s)}{G_{1v}(s)} \\ &= \frac{\left[m_t C_{ce} s^2 + \left(B_p C_{ce} + A_1 A_2\right) s + K C_{ce}\right]\left(\frac{s^2}{\omega^2} + \frac{2\zeta}{\omega} s + 1\right)}{K_{axv} K_1 \left(m_t s^2 + B_p s + K\right)} \end{aligned} \tag{38}$$

In the actual force control system, the signal of pressure sensor is analog voltage signal, which has the problem of high frequency noise. Although the second order Butterworth filtering method is used to filter the collected signal, the compensation voltage of the pressure signal still fluctuated sharply through the second order and above differential link. Therefore, the controller can be simplified by ignoring the compensations of the pressure sensor above the second order. This method can minimize the influence of pressure on the system control.

Eq. (38) can be reduced to the form as (39), shown at the bottom of the page.

Combining with Eqs. (33) and (34), the compensation item above the second order of the position sensor is ignored, then the system position load compensation controller $G_{xc1}(s)$ can be expressed as follows:

$$G_{xc1}(s) = \frac{\left(\frac{2A_1\zeta}{\omega} s^2 + A_{p1} s\right)}{K_{axv} K_1} \tag{40}$$

b: THE LOAD COMPENSATION CONTROL METHOD OF ROD CAVITY PRESSURE CONTROL SYSTEM

A method similar to section III (A) can be used to obtain the closed-loop control schematic diagram of the rod cavity pressure of the asymmetric cylinder, as shown in Figure 9.

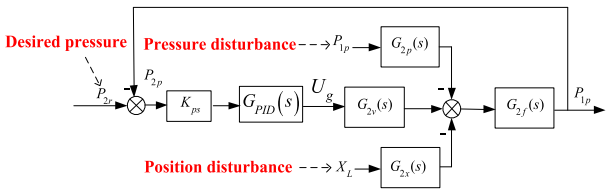

FIGURE 9. Schematic diagram of closed-loop control system of rod cavity pressure.

In the diagram above, P_{2r} is the desired pressure of the rod cavity's pressure control system, P_{2p} is the actual output pressure of the rod cavity's pressure control system, P_{1p} is asymmetrical cylinder without rod cavity actual

$$\frac{P_1}{X_L} = -G_{1x}(s)G_{1f}(s) = -\frac{-A_1 X_L s(m_t s^2 + B_p s + K)}{\frac{V_1 m_t}{\beta_e} s^3 + \left(C_{ce} m_t + \frac{V_1 B_p}{\beta_e}\right) s^2 + \left(A_1^2 + C_{ce} B_p + \frac{V_1 K}{\beta_e}\right) s + K C_{ce}} \tag{29}$$

$$\frac{P_1}{P_2} = -G_{1p}(s)G_{1f}(s) = \frac{-C_{ce}(m_t s^2 + B_p s + K) + A_1 A_2 s}{\frac{V_1 m_t}{\beta_e} s^3 + \left(C_{ce} m_t + \frac{V_1 B_p}{\beta_e}\right) s^2 + \left(A_1^2 + C_{ce} B_p + \frac{V_1 K}{\beta_e}\right) s + K C_{ce}} \tag{30}$$

$$\frac{P_1}{U_g} = G_{1v}(s)G_{1f}(s) = \frac{K_{axv} K_1 (m_t s^2 + B_p s + K)}{\left(\frac{s^2}{\omega^2} + \frac{2\zeta}{\omega} s + 1\right)\left[\frac{V_1 m_t}{\beta_e} s^3 + \left(C_{ce} m_t + \frac{V_1 B_p}{\beta_e}\right) s^2 + \left(A_1^2 + C_{ce} B_p + \frac{V_1 K}{\beta_e}\right) s + K C_{ce}\right]} \tag{31}$$

$$G_{pc1}(s) = \frac{\left[m_t C_{ce} + \frac{2KC_{ce}\zeta}{\omega} + \left(B_p C_{ce} + A_1 A_2\right)\frac{2\zeta}{\omega}\right] s^2 + \left[\frac{2KC_{ce}\zeta}{\omega} m_t C_{ce} + \left(B_p C_{ce} + A_{p1} A_{p2}\right)\right] s + K C_{ce}}{K_{axv} K_1 \left(m_t s + B_p + K\right)} \tag{39}$$

pressure output, $G_{2v}(s)$ and $G_{2f}(s)$ are the transfer functions of the rod cavity's pressure control system, $G_{2x}(s)$ is the transfer function of the external disturbance position to the pressure control system, $G_{2p}(s)$ is the transfer function of the rodless cavity's pressure acting on the pressure control system.

Combining with Eq. (27) and Eq. (22), the rod cavity pressure P_{2p} can be obtained as follows:

$$P_{2p} = \frac{Q_{sq2}+C_{ce}P_2-A_2X_Ps}{C_{ce}+\frac{V_2s}{\beta_e}} \tag{41}$$

Denoting $U_g = 0$ and $P_{2p} = 0$, according to Figure 9, v $G_{2x}(s)G_{2f}(s)$ can be obtained, the following equation can be obtained by inserting Eq. (41) to Eq. (24).

$$\begin{aligned}&\frac{P_{2p}}{X_L}\\&= -G_{2x}(s)G_{2f}(s)\\&= -\frac{-A_2X_Ls(m_ts^2+B_ps+K)}{\frac{V_2m_t}{\beta_e}s^3+\left(C_{ce}m_t+\frac{V_2B_p}{\beta_e}\right)s^2+\left(A_2^2+C_{ce}B_p+\frac{V_2K}{\beta_e}\right)s+KC_{ce}}\end{aligned} \tag{42}$$

Denoting $U_g = 0$ and $X_L = 0$, according to Figure 9, $G_{2p}(s)G_{2f}(s)$ can be obtained as follows.

$$\begin{aligned}&\frac{P_{1p}}{P_{2p}}\\&= -G_{2p}(s)G_{2f}(s)\\&= \frac{-C_{ce}(m_ts^2+B_ps+K)+A_1A_2s}{\frac{V_2m_t}{\beta_e}s^3+\left(C_{ce}m_t+\frac{V_2B_p}{\beta_e}\right)s^2+\left(A_2^2+C_{ce}B_p+\frac{V_2K}{\beta_e}\right)s+KC_{ce}}\end{aligned} \tag{43}$$

Donating $P_{1p} = 0$ and $X_L = 0$, according to Figure 9, $G_{2v}(s)G_{2f}(s)$ can be obtained as (44), shown at the bottom of the page.

According to Figure 6, the following equation can be obtained.

$$G_{2x}(s) = A_2\left(m_ts^3+B_ps^2+Ks\right) \tag{45}$$

The following equations can be obtained by combining with Eqs. (42) to (45)

$$\begin{aligned}&G_{2v}(s)\\&= K_2\left(m_ts^2+B_ps+K\right)\frac{K_{axv}}{\frac{s^2}{\omega^2}+\frac{2\zeta}{\omega}s+1}\end{aligned} \tag{46}$$

$$\begin{aligned}&G_{2p}(s)\\&= m_tC_{ce}s^2+\left(B_pC_{ce}+A_1A_2\right)s+KC_{ce}\end{aligned} \tag{47}$$

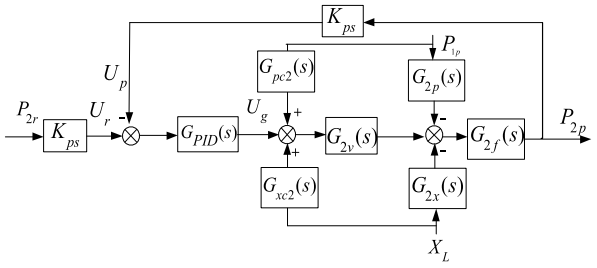

FIGURE 10. Schematic diagram of load compensation control of rod cavity pressure control system.

$$\begin{aligned}&G_{2f}(s)\\&= \frac{1}{\frac{V_2m_t}{\beta_e}s^3+\left(C_{ce}m_t+\frac{V_2B_p}{\beta_e}\right)s^2+\left(A_2^2+C_{ce}B_p+\frac{V_2K}{\beta_e}\right)s+KC_{ce}}\end{aligned} \tag{48}$$

Similarly, position load compensation controller $G_{xc2}(s)$ and pressure load compensation controller $G_{pc2}(s)$ of the pressure control system of rod cavity can be designed, and the compensation principle of the rod cavity's pressure control is shown in Figure 10.

$$\text{Assuming, } G_{pc2}(s) = \frac{G_{2p}(s)}{G_{2c}(s)} \tag{49}$$

$$G_{xc2}(s) = \frac{G_{2x}(s)}{G_{1v}(s)} \tag{50}$$

Combined with Eqs. (46) and (47), the controller is simplified by ignoring the compensation term of the pressure sensor higher than the second order, and the influence of pressure on system control is minimized. Then the system pressure load compensation controller G_{pc2} can be expressed as follows:

$$\begin{aligned}&G_{pc2}(s)\\&= \frac{G_{1p}(s)}{G_{1v}(s)}\\&= \frac{\left[m_tC_{ce}s^2+\left(B_pC_{ce}+A_1A_2\right)s+KC_{ce}\right]\left(\frac{s^2}{\omega^2}+\frac{2\zeta}{\omega}s+1\right)}{K_{axv}K_2\left(m_ts^2+B_ps+K\right)}\end{aligned} \tag{51}$$

Combined with Eqs. (45) and (46), and ignoring the compensation term of the position sensor higher than second order, the system position load compensation controller $G_{xc2}(s)$ can be expressed as follows:

$$G_{xc2}(s) = \frac{\frac{2A_{p2}\zeta}{\omega}s^2+A_{p2}s}{K_{axv}K_1} \tag{52}$$

$$\frac{P_{1p}}{U_g} = G_{1v}(s)G_{1f}(s) = \frac{K_{axv}K_2(m_ts^2+B_ps+K)}{\left(\frac{s^2}{\omega^2}+\frac{2\zeta}{\omega}s+1\right)\left[\frac{V_2m_t}{\beta_e}s^3+\left(C_{ce}m_t+\frac{V_2B_p}{\beta_e}\right)s^2+\left(A_2^2+C_{ce}B_p+\frac{V_2K}{\beta_e}\right)s+KC_{ce}\right]} \tag{44}$$

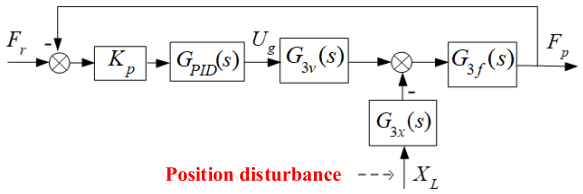

FIGURE 11. The control schematic diagram of force control system in simplified pump control loop.

2) LOAD COMPENSATION CONTROLLER FOR PUMP CONTROL LOOP

When analyzing the principle of the force control system of pump control loop, it is assumed that the servo valve or the pressurized fuel tank don't participate in the related control of the force control system, and the whole force control system is completed by the pump control loop. At this point, the function of the servo valve or the pressurized tank is to drain the excess flow caused by the asymmetrical flow of the left and right sides of the asymmetrical cylinder and to compensate the leaking oil of the system. Combined with the pump-control asymmetrical cylinder part in Figure 6, the influence of the servo valve and the pressurized tank on the system by filling or draining oil is ignored. For the convenience of the study, the control principle of the pump control loop force control system is obtained, as shown in Figure 11.

For the sake of calculation, some equations in Figure 6 are transformed as follows:

$$A = C_{ip} + \frac{V_1}{\beta_e} s \tag{53}$$

$$B = -C_{ip} - \frac{V_2}{\beta_e} s \tag{54}$$

Combining with Eq. (53), Eq. (54), Eq. (21) and Eq. (22), two cavity pressure of asymmetrical cylinder P_{1p} and P_{2p} can be obtained as follows.

$$P_{1p} = \frac{Q_{f1}B - A_1 X_p B s + C_{ce}(Q_{f2} - A_2 X_p s)}{C_{ce}^2 + AB} \tag{55}$$

$$P_{2p} = \frac{Q_{f2}A - A_2 X_p A s - C_{ce}(Q_{f1} - A_1 X_p s)}{C_{ce}^2 + AB} \tag{56}$$

Denoting $U_g = 0$, according to Figure 11, $G_{3x}(s)G_{3f}(s)$ can be obtained as follows by inserting Eqs. (55) and (56) into Eq. (24), (57), as shown at the bottom of the page.

Denoting $X_L = 0$, according to Figure 11, $G_{3v}(s)G_{3f}(s)$ can be obtained as follows

$$\begin{aligned}\frac{F_p}{U_g} &= G_{3v}(s)\, G_{3f}(s) \\ &= \frac{\frac{D_p K_V K_{PI} K (V_2 A_1 + V_1 A_2)}{\beta_e [LJ^2 s^2 + RJ^2 s + J(K_c K_t + K_{PI} K_f)]} (m_t s^2 + B_p s + K)}{\left\{ \begin{array}{l} \frac{m_t V_1 V_2}{\beta_e^2} s^4 + \frac{B_p V_1 V_2 + \beta_e C_{ip} m_t (V_1 + V_2)}{\beta_e^2} s^3 \\ + \frac{\beta_e (V_2 A_1^2 + V_1 A_2^2 + B_p C_{ip} (V_1 + V_2)) + K V_1 V_2}{\beta_e^2} s^2 \\ + C_{ip} \left((A_1 - A_2)^2 + \frac{K C_{ip} (V_1 + V_2)}{\beta_e} \right) s \end{array} \right\}}\end{aligned} \tag{58}$$

According to Figure 6, the following equation can be obtained.

$$G_{3x}(s) = \left[\frac{(V_2 A_1^2 + V_1 A_2^2)}{\beta_e} s^2 + C_{ip} (A_1 - A_2)^2 s \right] (m_t s^2 + B_p s + K) \tag{59}$$

The following equations can be obtained by combining with Eqs. (57) to (59), (60) and (61), as shown at the bottom of the next page.

Combined with Figure 11, when the external disturbance position X_L acts on the force control system of the pump control loop, the output F_p of the force control system will be affected to some extent. By designing position load compensation controller $G_{xc3}(s)$, the influence of external position disturbance on force control system of pump control loop can be eliminated or weakened. The load compensation control principle of force control system of pump control loop is shown in Figure 12.

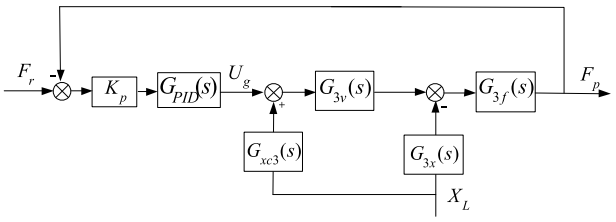

FIGURE 12. The load compensation control schematic diagram of force control system of pump control loop.

Making an assumption as follows:

$$G_{xc3}(s) = \frac{G_{3x}(s)}{G_{3v}(s)} \tag{62}$$

$$\frac{F_p}{X_L} = -G_{1p}(s)G_{2p}(s) = -\frac{\left[\frac{(V_2 A_{p1}^2 + V_1 A_{p2}^2)}{\beta_e} s^2 + C_{ip} \left(A_{p1} - A_{p2}\right)^2 s \right] (m_t s^2 + B_p s + K)}{\frac{m_t V_1 V_2}{\beta_e^2} s^4 + \frac{B_{p1} V_1 V_2 + \beta_e C_{ip} m_{t1} (V_1 + V_2)}{\beta_e^2} s^3 + \frac{\beta_e (V_2 A_{p1}^2 + V_1 A_{p2}^2 + B_{p1} C_{ip} (V_1 + V_2)) + K V_1 V_2}{\beta_e^2} s^2 + C_{ip} \left((A_{p1} - A_{p2})^2 + \frac{K C_{ip} (V_1 + V_2)}{\beta_e} \right) s} \tag{57}$$

Combined with Eqs. (59) and (60), the system position load compensation controller $G_{xc3}(s)$ can be expressed as follows:

$$G_{xc3}(s) = \frac{C_{ip}RJ^2\left(A_{p1}-A_{p2}\right)^2 s^2+J\left(K_cK_t+K_{PI}K_f\right)C_{ip}\left(A_{p1}-A_{p2}\right)^2}{\frac{D_pK_VK_{PI}K_t(V_2A_{p1}+V_1A_{p2})}{\beta_e}} \tag{63}$$

B. COMPENSATION CONTROL METHOD FOR TRACKING ERROR IN FORCE CONTROL SYSTEM

1) TRACKING ERROR COMPENSATION CONTROLLER FOR VALVE CONTROL LOOP

The load compensation controller designed in section III-A can greatly reduce or even eliminate the influence of external load disturbance on the pressure control accuracy. Although the output of the pressure control system after compensation is not affected by external load disturbance. In fact, there is still a tracking error between the output pressure and the input pressure of the pressure control system. This error not only directly affects the control accuracy of the pressure control system, but also affects the control accuracy of the whole force control system.

In this section, aimed at the pressure control system of rodless cavity, force tracking error compensation controller $G_{ff1}(s)$ is introduced, which can weaken or even eliminate the system tracking error. At this point, the influence of external load disturbance on the rodless cavity pressure closed-loop control system is ignored, and the tracking error compensation principle of the rodless cavity's pressure control system is shown in Figure 13.

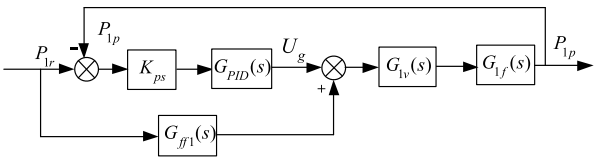

FIGURE 13. The schematic diagram of the tracking error compensation of the rodless cavity's pressure control system.

The pressure closed-loop transfer function of rodless cavity can be expressed as follows:

$$\Phi_d(s) = \frac{P_{1p}}{P_{1r}} = \frac{K_pG_{PID}G_{1v}(s)G_{1f}(s)}{1+K_pG_{PID}G_{1v}(s)G_{1f}(s)} \tag{64}$$

Supposing the force tracking error compensation controller's transfer function is $G_{ff}(s) = 1/G_{1v}(s)G_{1f}(s)$, and its systematic error is $E(s) = (1-\Phi_d(s))R(s) = 0$, this method theoretically eliminates the tracking error caused by the input signal and achieves complete compensation control.

Ignoring the influence of higher order terms above the second order, the tracking error compensation controller $G_{ff1}(s)$ can be expressed as (65), shown at the bottom of the next page.

Similarly, aimed at the pressure control system of rod cavity, the force tracking error compensation controller $G_{ff2}(s)$ is introduced to eliminate or even weaken the system tracking error. The tracking error compensation principle of the rod cavity pressure control system is shown in Figure 14.

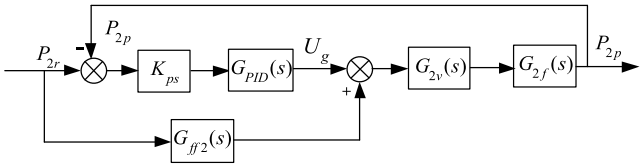

FIGURE 14. The schematic diagram of rod cavity pressure control system's tracking error compensation.

The derivation process of the tracking error compensation controller $G_{ff2}(s)$ of the pressure control system with bar cavity is similar to that of $G_{ff1}(s)$. Ignoring the influence of the higher-order terms above the second order, the force tracking error compensation controller $G_{ff2}(s)$ can be expressed as (66), shown at the bottom of the next page.

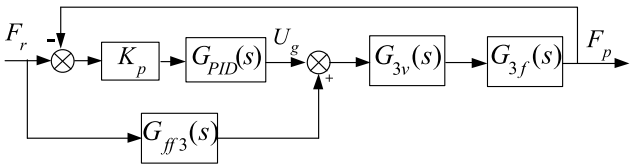

FIGURE 15. The schematic diagram of pump control loop tracking error compensation control system.

2) THE TRACKING ERROR COMPENSATION CONTROLLER OF PUMP CONTROL LOOP

In this section, for the force control system of pump control loop, the tracking error compensation controller $G_{ff3}(s)$ is introduced to reduce or even eliminate the tracking error of the system, and the influence of external position disturbance on the force control system is ignored. The principle diagram of tracking error compensation control for the pump control loop is shown in Figure 15.

The derivation process of the tracking error compensation controller $G_{ff3}(s)$ for the pump control loop is similar to that of $G_{ff1}(s)$. By ignoring the effects of higher order terms

$$G_{3v}(s) = \frac{D_p(V_2A_1+V_1A_2)K_VK_{PI}K_t}{\beta_e}\frac{(m_ts^2+B_ps+K)}{LJ^2s^3+RJ^2s^2+J\left(K_cK_t+K_{PI}K_f\right)} \tag{60}$$

$$G_{3f}(s) = \frac{1}{\frac{m_tV_1V_2}{\beta_e^2}s^4+\frac{B_pV_1V_2+\beta_eC_{ip}m_t(V_1+V_2)}{\beta_e^2}s^3+\frac{\beta_e(V_2A_1^2+V_1A_2^2+B_pC_{ip}(V_1+V_2))+KV_1V_2}{\beta_e^2}s^2}+C_{ip}\left((A_1-A_2)^2+\frac{KC_{ip}(V_1+V_2)}{\beta_e}\right)s \tag{61}$$

above the second order, the force tracking error compensation controller $G_{ff3}(s)$ can be expressed as follows.

$$G_{ff3}(s) = \frac{1}{G_{1p}(s)\,G_{1p}(s)} \left\{ \begin{array}{l} \dfrac{\beta_e J\left(K_c K_t + K_{PI} K_f\right)\left[V_2 A_{p1}^2 + V_1 A_{p2}^2 + B_{p1} C_{ip}(V_1+V_2)\right]}{\beta_e^2} \\ + C_{ip} R J^2 \left(A_{p1} - A_{p2}\right)^2 \end{array} \right\} s^2 + \left\{ J C_{ip} \left(A_{p1} - A_{p2}\right)^2 \left(K_c K_t + K_{PI} K_f\right) \right\} s = \frac{}{\frac{D_p K_V K_{PI} K (V_2 A_{p1} + V_1 A_{p2})}{\beta_e} (m_t s^2 + B_p s + K)} \tag{67}$$

V. EXPERIMENT

A. INTRODUCTION OF EXPERIMENTAL PLATFORM OF PCDS

In order to further study the performance of PCDS force control, a PCDS performance test platform is designed, and the schematic diagram is shown in Figure 16.

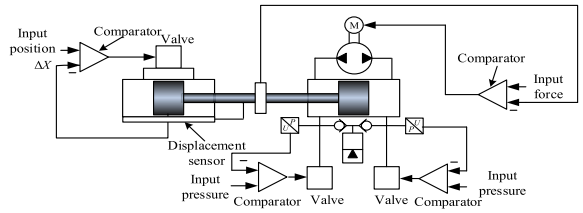

a) Schematic diagram of PCDS performance test platform

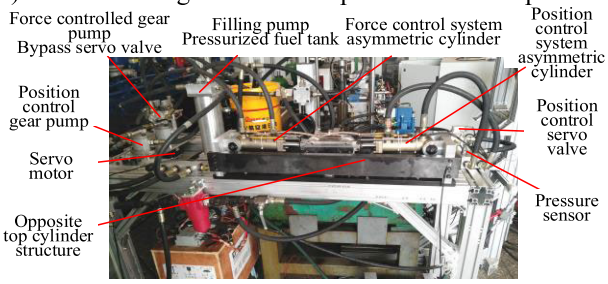

b) Physical diagram of PCDS performance test platform

FIGURE 16. PCDS performance test platform.

Fig. 16a adopts the principle of electro-hydraulic force simulator [25], which is widely used in aerospace, ship, engineering machinery and many other fields. Two sets of hydraulic actuators are installed opposite each other. The right part is PCDS, which is composed of asymmetrical cylinder, servo motor, gear pump, servo valve and pressure sensor. The actual force output of the system is obtained by calculating the pressure of asymmetrical two cavities, Left part is the valve-controlled cylinder position control system, which is the loading system of PCDS. It is made up of flow servo valve, asymmetrical cylinder, position sensor and so on. The position control system and the system to be tested are rigidly connected by a mass block. Two systems use the same type of asymmetrical cylinder. The physical diagram of PCDS performance test platform is shown in Figure 16b.

B. EXPERIMENTAL PLAN

1) EXPERIMENTAL SCHEME OF TRACKING ERROR COMPENSATION CONTROL METHOD

Since the current experimental platform is in the valve oil-drain drive mode mentioned in section I, the servo valve only can be used for oil drain and cannot supply oil to the two cavities of the asymmetric cylinder. Meanwhile, because the actual system pressure is lower than the desired pressure in the two-cavity pressure control of the non-symmetrical cylinder, the servo valve is needed to supply oil to the two cavities of the non-symmetrical cylinder. However, such experimental condition isn't available in our lab at present. So the experimental effect of the tracking error compensation control method for valve control loop cannot be verified at present. Therefore, the tracking error compensation experiment only verifies the tracking error compensation control method of the pump-control system.

Typical sinusoidal force tracking signals are input to the force control system, and the given signal of load simulation system is set as a constant. The specific experimental conditions are shown in Table 1.

2) EXPERIMENTAL SCHEME OF LOAD COMPENSATION CONTROL METHOD

In order to verify the disturbance rejection performance of the load compensation control method proposed in this paper, the given force signal of the force control system is set as a constant, and the typical sinusoidal position disturbance

$$G_{ff1}(s) = \frac{1}{G_{1v}(s)\,G_{1f}(s)} = \frac{\left[\begin{array}{l} \dfrac{V_1 m_t}{\beta_e} s^3 + \left(C_{ce} m_t + \dfrac{V_1 B_p}{\beta_e}\right) s^2 \\ + \left(A_1^2 + C_{ce} B_p + \dfrac{V_1 K}{\beta_e}\right) s + K C_{ce} \end{array}\right] \left(\frac{s^2}{\omega^2} + \frac{2\zeta}{\omega} s + 1\right)}{K_{axv} K_1 X_v (m_t s^2 + B_p s + K)} \tag{65}$$

$$G_{ff2}(s) = \frac{\left[\left(C_{ce} m_t + \frac{V_2 B_p}{\beta_e}\right) + \frac{2\zeta}{\omega}\left(A_{p2}^2 + C_{ce} B_p + \frac{V_2 K}{\beta_e}\right) + \frac{K C_{ce}}{\omega^2}\right] s^2 + \left[\left(A_{p2}^2 + C_{ce} B_p + \frac{V_2 K}{\beta_e}\right) + \frac{2\zeta K C_{ce}}{\omega}\right] s + K C_{ce}}{K_{axv} K_2 X_v (m_t s^2 + B_p s + K)} \tag{66}$$

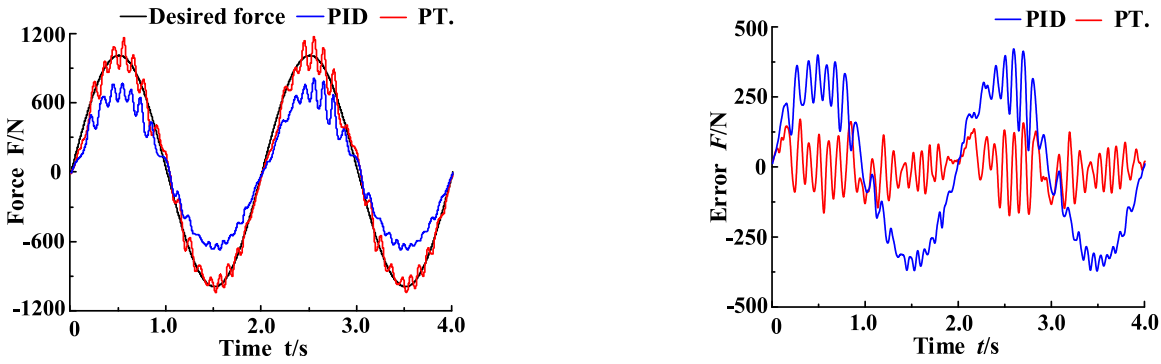

a) Force control response curve

b) Force error curve

FIGURE 17. Force input is 1000 N amplitude with the 0.5 Hz frequency and without position disturbance input.

TABLE 1. Experimental condition of tracking error compensation control method.

Experimental condition	Sinusoidal input force		Disturbance position
	Amplitude	Frequency	
①	1000 N	0.5 Hz	0 mm
②	2000 N	0.5 Hz	0 mm

TABLE 2. Experimental conditions of load disturbance control method.

Experimental condition	Input force	Sinusoidal disturbance position	
		Amplitude	Frequency
①	0 N	8 mm	1 Hz
②	0 N	12 mm	2 Hz

TABLE 3. Experimental conditions of compound control method.

Experimental condition	Sinusoidal input force		Sinusoidal disturbance position	
	Amplitude	Frequency	Amplitude	Frequency
①	1000 N	0.5 Hz	8 mm	1 Hz
②	2000 N	0.5 Hz	8 mm	1 Hz

signal of the load simulation system is given. Specific experimental conditions are shown in Table 2.

3) EXPERIMENTAL SCHEME OF COMPOUND COMPENSATION CONTROL METHOD

In order to verify the compensation effect of the compound control method combined with the tracking error compensation control method and the load compensation control method, a typical sinusoidal force tracking signal is given to the force control system, and the typical sinusoidal position disturbance of the load simulation system is given. The specific experimental conditions are shown in Table 3.

C. EXPERIMENTAL RESULT

This section will verify the effect of the control method from three parts: load compensation control method, the tracking error compensation control method and compound compensation control method. This section is designed to verify the effectiveness of the control methods of each loop respectively, and then the pump control loop and the valve control loop are combined to form the control method of the pump valve compound drive control, and the effect of the control method is verified.

1) EXPERIMENTAL VERIFICATION OF THE TRACKING ERROR COMPENSATION CONTROL METHOD

The force control response curve and force error curve in the experimental conditions shown in Table 1 are shown in Figure 17 and Figure 18 respectively. In the figures, PID represents the output force curve obtained by the force control system using a simple PID controller, and PT. represents the output force curve obtained by the tracking error compensation control method in the pump control loop. The reduction rate of maximum force error and the elimination rate of mean force error are selected as the evaluation indexes of its performance, as shown in Table 4.

The tracking conclusions can be obtained from Figure 17, Figure 18 and Figure 19. Under different working conditions, the tracking error compensation control method of the pump control loop can greatly reduce the force tracking error of the system and improve the tracking accuracy of PCDS force control. For example, in the situation that the sinusoidal force tracking signal of the system is 1000 N amplitude with 0.5Hz frequency, the maximum force error of the PID controller is about 412.28N. The maximum force error generated by the tracking error compensation control method of pump control loop is about 170.19N, which improves the accuracy of PID control by 58.72%. Meanwhile, the mean force error of the pump control loop is 216.63N, which improves the accuracy of PID control by 71.42%. The experimental results verify the validity of the tracking error compensation control method.

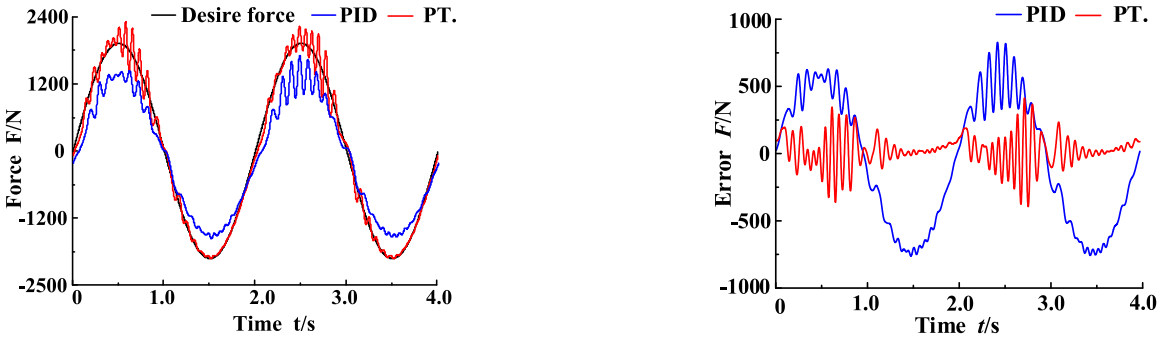

a) Force control response curve b) Force error curve

FIGURE 18. Force input is 2000 N amplitude with 0.5 Hz frequency and without position disturbance input.

TABLE 4. Performance indexes I of load compensation control method (%, reserved two decimal digits).

Evaluation indexes	Maximum force error (N)				Elimination rate of maximum force error (%)		
	PID	VL.	PL.	VL+PL	VL.	PL.	VL+PL
Experimental condition①	171.82	143.57	73.34	45.01	16.44	57.32	73.80
Experimental condition②	247.81	179.31	106.26	64.25	27.64	57.12	74.07

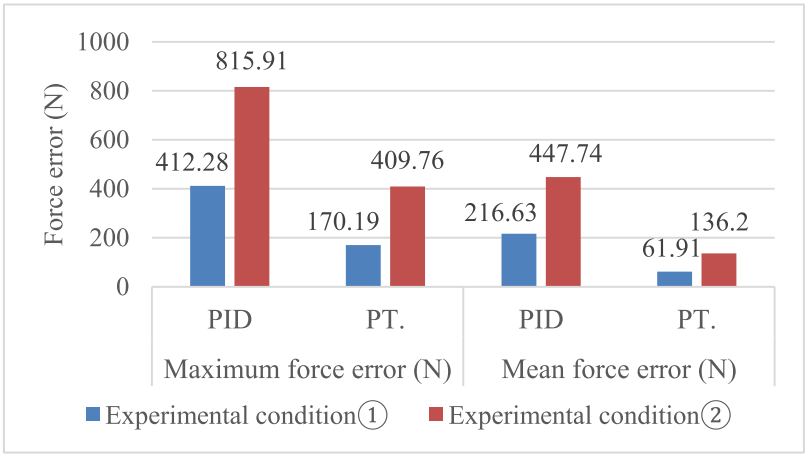

FIGURE 19. Performance indexes of tracking error compensation control method.

In general, under different sinusoidal force input conditions, the elimination rate of maximum force error of the system using the tracking error compensation control method is increased by more than 49% compared with PID, and the elimination rate of mean force error is increased by more than 70% compared with PID. This control method greatly improves the performance of force control.

2) EXPERIMENTAL VERIFICATION OF LOAD COMPENSATION CONTROL METHOD

In Table 2, the force control response curve and force error curve of each working condition are shown in Figure 20 and Figure 21. In the figures, PID represents the output force curve of force control system adopted a simple PID controller. VL. represents the output force curve adopted load compensation control method only in the valve control loop. PL. represents the output force curve adopted load compensation control method only in the pump control loop. PL +VL represents the output force curve adopted the load compensation control method in both the valve control loop and the pump control loop. The tables of performance evaluation indexes are made as shown in Table 4 and Table 5.

It can be seen from Figure 20, Figure 21, Table 4 and Table 5 that, under different working conditions, both the load compensation control method of the pump control loop and the load compensation control method of the valve

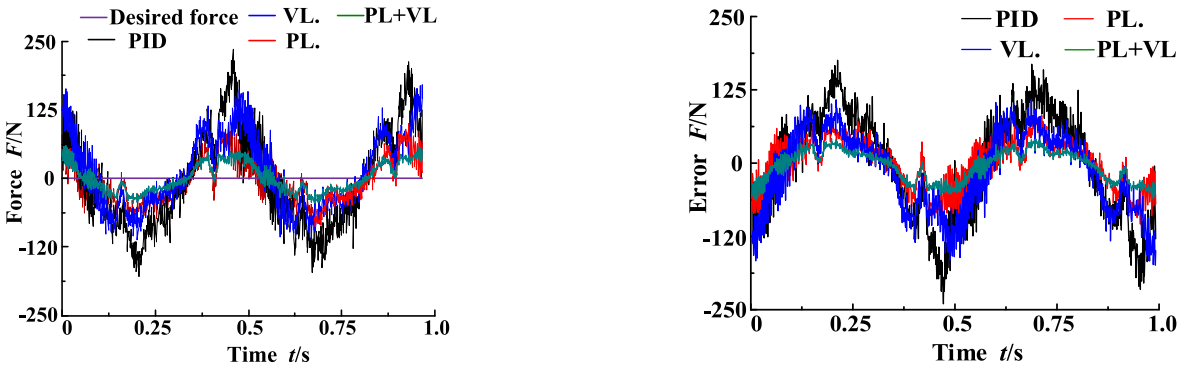

a) Force control response curve b) Force error curve

FIGURE 20. No input force, and the disturbance position is 8 mm amplitude with 2 Hz frequency.

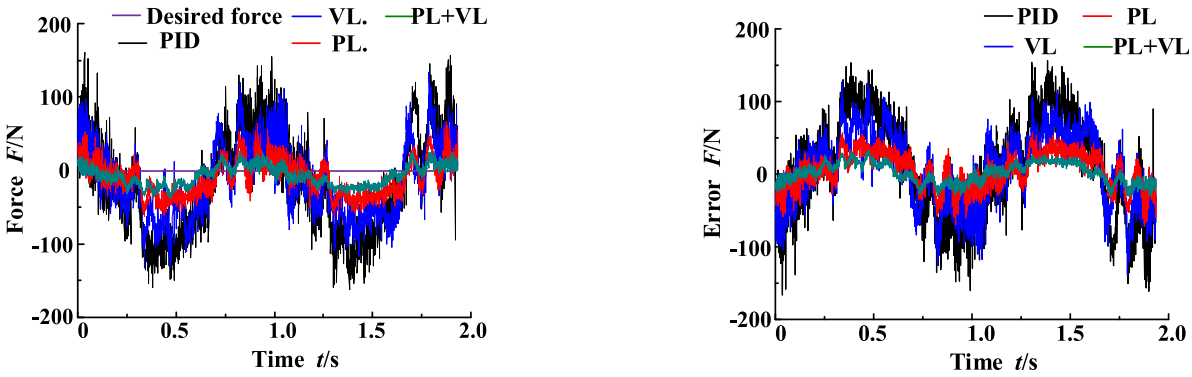

a) Force control response curve b) Force error curve

FIGURE 21. No input force, and the disturbance position is 12 mm amplitude with 1 Hz frequency.

TABLE 5. Performance indexes II of load compensation control method (%, reserved two decimal digits).

Evaluation indexes	Mean force error (N)				Elimination rate of mean force error (%)		
	PID	VL.	PL.	VL+PL	VL.	PL.	VL+PL
Experimental condition①	61.19	44.40	22.27	12.38	27.44	63.61	79.77
Experimental condition②	79.61	59.61	36.01	23.24	25.12	54.77	70.81

control loop have certain disturbance rejection ability and can improve the robustness of pump-valve compound drive force control system. For example, when the sinusoidal position disturbance signal inputted to the system is 12 mm amplitude with 2 Hz frequency, the maximum force error of the PID controller is about 247.81N, and the maximum force error generated by the load compensation control method of the valve control loop is about 179.31N. Compared with PID, its disturbance rejection ability is improved by 27.64%. The maximum force error produced by load compensation control method of pump-controlled loop is 106.26N, which is 57.12% higher than PID. When the valve-controlled load compensation control method is introduced based on the pump-controlled load compensation control method, the maximum force error is about 64.25N, which represents its disturbance rejection ability is improved by 74.07% compared with PID and is improved by 16.95% compared with pump-controlled loop load compensation control method. These experimental results verify the effectiveness of the load compensation control method in section III-A.

It is worth noting that only when the force control system is disturbed by high amplitude position disturbance, the error curve of the force control system changes obviously. After analyzing the reasons are as follows: the leakage of PCDS force control system is large. There are the following places to produce oil drain: the internal leakage of gear pump, servo

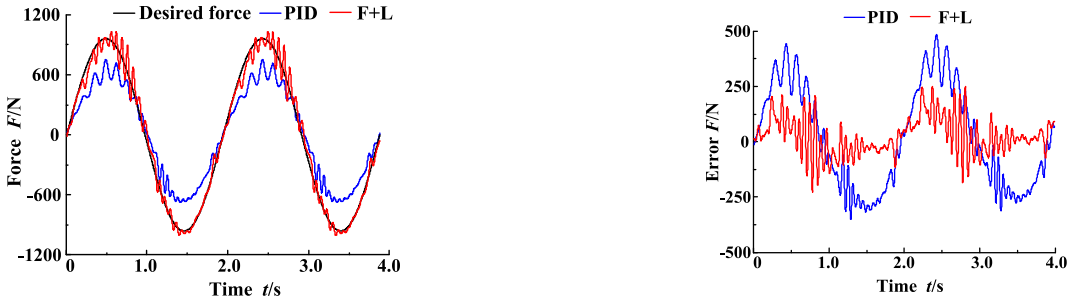

a) Force control response curve b) Force error curve

FIGURE 22. Force input is 1000N amplitude with 0.5Hz frequency, and the disturbance position of 8mm amplitude with 2Hz frequency.

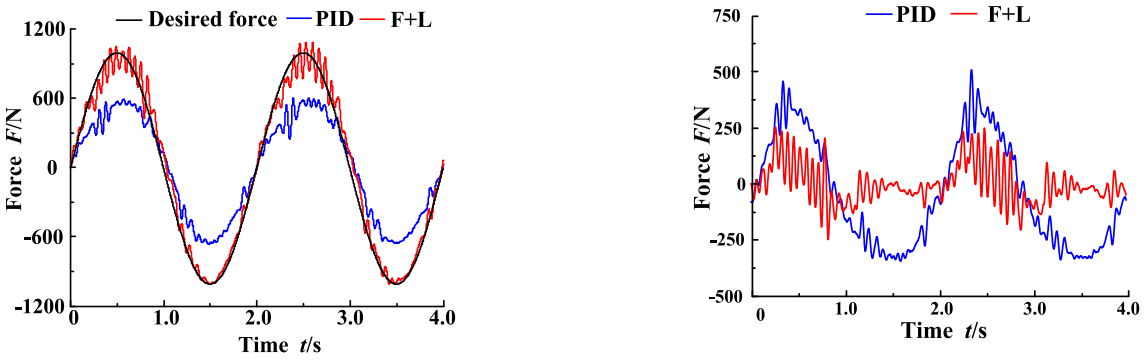

a) Force control response curve b) Force error curve

FIGURE 23. Force input is 1000N amplitude with 0.5Hz frequency, and the disturbance position of 12mm amplitude with 1Hz frequency.

TABLE 6. Performance indexes of the compound control method (%, reserved two decimal digits).

Evaluation indexes	Maximum force error (N)		Elimination rate of force error maximum (%)	Mean of the force error (N)		Elimination rate of mean of the force error (%)
	PID	F+L		PID	F+L	
Experimental condition①	632.47	256.60	59.42	240.58	65.07	72.95
Experimental condition②	458.83	254.90	44.44	213.18	66.09	68.99

valve pilot class at both ends of pump port and control valve spool. When external position disturbance is considered, the open-loop transfer function of the force control system is shown as follows:

$$F_p = \frac{\frac{D_p A_p w}{C_t}\left(\frac{s^2}{w_m}+\frac{2\xi_m}{w_m}s+1\right)}{\left(\frac{s}{w_r}+1\right)\left(\frac{s^2}{w_0}+\frac{2\xi_0}{w_0}s+1\right)}$$

It can be seen from Eq. (68) that, as the oil spills C_t increases, the denominator of the external position disturbance term increases, reducing the influence of the external position disturbance on the force control system finally.

To sum up, pump-valve compound drive force control system has good disturbance rejection ability. Meanwhile, adopting load error compensation control method, the load compensation control method of pump control loop increases by more than 57% compared with the PID disturbance rejection ability. Compared with the load compensation control method combined with the pump control loop and the valve control loop, its disturbance rejection capability is improved by about 68%. This further improves the disturbance rejection ability of force control and the robustness of force control.

3) EXPERIMENTAL VERIFICATION OF COMPOUND CONTROL METHOD FOR FORCE CONTROL SYSTEM

Force control response curve and force error curve showing in Figure 22 and Figure 23 are obtained under the

experimental condition showing in Table 3. In the figures, PID represents the output force curve of the force control system using a simple PID controller, and F+L represents the output force curve of the force control system using a compound control method combining the tracking error compensation control method and load compensation control method. The force error performance indexes of compound control method are made as shown in Table 6.

According to the Figure 22, Figure 23 and Table 6, it's observed that under different working conditions, the control accuracy of force control system adopted compound control method is increased by more than 44%. It largely improves tracking accuracy, disturbance rejection ability and force control performance. For example, under the condition that the sinusoidal force tracking signal is 1000 N amplitude with 0.5Hz frequency and the disturbance position is 8 mm amplitude with 1 Hz frequency, the maximum force error of the PID controller is about 458.83N. The maximum force error of compound control method is about 254.90N, which improves the accuracy of PID control by 44.44%. Therefore, the method designed for pump-valve compound drive force control system in this section has satisfied experimental effect, which verifies the validity of the theory in section III in this paper.

VI. CONCLUSION

Aimed at the demand of energy saving, high precision and high response speed for legged robot joint driver, PCDS is designed in this paper to improve the cruising ability in field work, and the mathematical model of nonlinear force control of the system is established. On this basis, the research on its force control method is conducted, and a force control method combining tracking error compensation and load compensation control is designed. The tracking error compensation control method, the load compensation control method and the force control method combined with the tracking error compensation and load compensation control are verified by a series of experiments on the PCDS performance testing platform. These methods are compared with the control method only used the simple PID, which verifies the effectiveness of the force control method combined with the tracking error compensation and load compensation control. Through the research in this paper, the following achievements and conclusions are obtained as follows:

Firstly, the designed PCDS is divided into three parts: pump control loop, valve control loop and oil-addition loop. The output force of the whole system can be controlled by the force closed-loop control of pump control loop and the pressure closed-loop control of the two-cavity of asymmetric cylinder, which improves the energy efficiency of a single valve-controlled cylinder and response speed, the control accuracy of a single pump-control cylinder. This makes PCDS achieve better control performance with faster response, higher precision and lower energy loss.

Secondly, the mathematical model of PCDS force control system is established, considering the factors of system servo valve pressure-flow nonlinearity, servo cylinder asymmetry and load complexity and variability. And the mathematical model of the pump control loop of the system is simplified, which lays a theoretical foundation for the research of the relevant controller.

Thirdly, a force control method combining the tracking error compensation and load compensation control is designed and is verified on the PCDS test platform. The experimental results show that the PCDS can meet the requirements of high precision, high response and energy saving for the hydraulic drive unit of the legged robot joint. The designed load compensation control method can effectively suppress the influence of external position disturbance on the tracking accuracy of the force control system. Compared with PID, it can improve the control accuracy by approximately 49% and the tracking error compensation control method can effectively improve the tracking accuracy of the force control system by more than 68%.

REFERENCES

[1] Z. Luo, J. Shang, G. Wei, and L. Ren, "Module-based structure design of wheeled mobile robot," *Mech. Sci.*, vol. 9, no. 1, pp. 103–121, Feb. 2018.

[2] Q. Liu, J. Zhao, H. Zhu, G. Wang, and J. D. McLennan, "Review, classification and structural analysis of downhole robots: Core technology and prospects for application," *Robot. Auto. Syst.*, vol. 115, pp. 104–120, May 2019.

[3] O. Y. Kanner, N. Rojas, L. U. Odhner, and A. M. Dollar, "Adaptive legged robots through exactly constrained and non-redundant design," *IEEE Access*, vol. 5, pp. 11131–11141, 2017.

[4] M. Nakajima, M. Tanaka, K. Tanaka, and F. Matsuno, "Motion control of a snake robot moving between two non-parallel planes," *Adv. Robot.*, vol. 32, no. 10, pp. 559–573, May 2018.

[5] S. Pan, L. Shi, and S. Guo, "A Kinect-based real-time compressive tracking prototype system for amphibious spherical robots," *Sensors*, vol. 15, no. 4, pp. 8232–8252, Apr. 2015.

[6] L. Lyu, Z. Chen, and B. Yao, "Advanced valves and pump coordinated hydraulic control design to simultaneously achieve high accuracy and high efficiency," *IEEE Trans. Control Syst. Technol.*, early access, Feb. 25, 2020, doi: 10.1109/TCST.2020.2974180.

[7] L. Lyu, Z. Chen, and B. Yao, "Development of pump and valves combined hydraulic system for both high tracking precision and high energy efficiency," *IEEE Trans. Ind. Electron.*, vol. 66, no. 9, pp. 7189–7198, Sep. 2019.

[8] B. Baigzadehnoe, Z. Rahmani, A. Khosravi, and B. Rezaie, "On position/force tracking control problem of cooperative robot manipulators using adaptive fuzzy backstepping approach," *ISA Trans.*, vol. 70, pp. 432–446, Sep. 2017.

[9] J. Li, Y. Wang, X. Wang, J. Shao, T. Yang, and Z. Mao, "Research on electro-hydraulic force servo system based on neural network and fuzzy intelligent control strategy," *J. Comput. Theor. Nanosci.*, vol. 11, no. 4, pp. 1205–1210, Apr. 2014.

[10] K. K. Ahn and Q. T. Dinh, "Self-tuning of quantitative feedback theory for force control of an electro-hydraulic test machine," *Control Eng. Pract.*, vol. 17, no. 11, pp. 1291–1306, Nov. 2009.

[11] S. Wen, J. Zhu, X. Li, A. B. Rad, and X. Chen, "End-point contact force control with quantitative feedback theory for mobile robots," *Int. J. Adv. Robot. Syst.*, vol. 9, no. 6, p. 236, Dec. 2012.

[12] F. Zhou, Y. Li, and G. Liu, "Robust decentralized force/position fault-tolerant control for constrained reconfigurable manipulators without torque sensing," *Nonlinear Dyn.*, vol. 89, no. 2, pp. 955–969, Jul. 2017.

[13] S. Oh and K. Kong, "High-precision robust force control of a series elastic actuator," *IEEE/ASME Trans. Mechatronics*, vol. 22, no. 1, pp. 71–80, Feb. 2017.

[14] T. Endo, F. Matsuno, and H. Kawasaki, "Force control and exponential stabilisation of one-link flexible arm," *Int. J. Control*, vol. 87, no. 9, pp. 1794–1807, Sep. 2014.

[15] J. Yao, Z. Jiao, and B. Yao, "Nonlinear adaptive robust backstepping force control of hydraulic load simulator: Theory and experiments," *J. Mech. Sci. Technol.*, vol. 28, no. 4, pp. 1499–1507, Apr. 2014.

[16] Z. Wang, R. Duan, G. Sun, and M. Chi, "Hydraulic quadruped robot joint force control based on double internal model controller," *Int. J. Control Autom.*, vol. 9, no. 1, pp. 241–250, Jan. 2016.

[17] Q. L. Cao, S. R. Li, and D. Y. Zhao, *Adaptive Motion/Force Control of Constrained Manipulators Using a New Fast Terminal Sliding Mode*. Geneva, Switzerland: Inderscience Publishers, Jun. 2014, pp. 150–156.

[18] J. Yao, Z. Jiao, B. Yao, Y. Shang, and W. Dong, "Nonlinear adaptive robust force control of hydraulic load simulator," *Chin. J. Aeronaut.*, vol. 25, no. 5, pp. 766–775, Oct. 2012.

[19] D. Q. Truong and K. K. Ahn, "Force control for hydraulic load simulator using self-tuning grey predictor–fuzzy PID," *Mechatronics*, vol. 19, no. 2, pp. 233–246, Mar. 2009.

[20] P. Nakkarat and S. Kuntanapreeda, "Observer-based backstepping force control of an electrohydraulic actuator," *Control Eng. Pract.*, vol. 17, no. 8, pp. 895–902, Aug. 2009.

[21] K. Ba, B. Yu, X. Kong, C. Li, Q. Zhu, H. Zhao, and L. Kong, "Parameters sensitivity characteristics of highly integrated valve-controlled cylinder force control system," *Chin. J. Mech. Eng.-EN*, vol. 31, no. 1, p. 43, May 2018.

[22] K. Ba, B. Yu, Z. Gao, Q. Zhu, G. Ma, and X. Kong, "An improved force-based impedance control method for the HDU of legged robots," *ISA Trans.*, vol. 84, pp. 187–205, Jan. 2019.

[23] K.-X. Ba, G.-L. Ma, B. Yu, Z.-G. Jin, Z.-P. Huang, J.-X. Zhang, and X.-D. Kong, "A nonlinear model-based variable impedance parameters control for position-based impedance control system of hydraulic drive unit," *Int. J. Control, Autom. Syst.*, vol. 18, no. 7, pp. 1806–1817, Jul. 2020, doi: 10.1007/s12555-019-0151-0.

[24] S. Habibi and A. Goldenberg, "Design of a new high-performance electrohydraulic actuator," *IEEE/ASME Trans. Mechatronics*, vol. 5, no. 2, pp. 158–164, Jun. 2000.

[25] C. Luo, J. Yao, F. Chen, L. Li, and Q. Xu, "Adaptive repetitive control of hydraulic load simulator with RISE feedback," *IEEE Access*, vol. 5, pp. 23901–23911, 2017.